Controlling Microbial Adhesion to the Surfaces Using Topographical Cues

Mehdi Kargar

Thesis submitted to the faculty of the Virginia Polytechnic Institute and State University
in partial fulfillment of the requirements for the degree of

Master of Science
In
Mechanical Engineering

Bahareh Behkam, Chair
Amrinder S. Nain
Mark R. Paul

May 08, 2013
Blacksburg, VA

Keywords: Bioadhesion, Soft membrane, *Pseudomonas aeruginosa*, Nanofibers

Controlling Microbial Adhesion to the Surfaces Using Topographical Cues

Mehdi Kargar

ABSTRACT

The state of adhesion of bacteria to nanofiber-textured model surfaces is analyzed at single-cell level. The results reveal similarities between the effect of topography on bacteria-surface interactions and vesicle-surface interactions. The results are discussed in the context of controlling bacterial adhesion to surfaces using nanofibrous topographical features.

Acknowledgements

This work was partially funded by the Jeffress Memorial Trust and the Virginia Tech's Institute for Critical Technology and Applied Sciences (ICTAS). We thank Dr. Florian Schubot (Biological Sciences, Virginia Tech) for providing us with the microorganism. We are thankful for insightful discussions with the Laboratory for Interdisciplinary Statistical Analysis (LISA) and the following faculty members at Virginia Tech: William Ducker (Chemical Engineering), Zhaomin Yang (Biological Sciences), and Xinwei Deng (Statistics). We appreciate the help of Jeffrey Saucke, Mohsen Gheisarieha, Hodjat Pendar, and Amy Tillman with the experiments and analysis.

The results of this thesis was published in "Soft Matter" journal[1] with Mr. Ji Wang, professor Amrinder S. Nain and professor Bahareh Behkam as co-authors.

Table of contents

List of figures

List of tables

Chapter 1. Introduction

Adhesion of microorganisms to surfaces is the starting point of the formation of complex microbial societies known as biofilm. Depending on the application, bio-adhesion and biofilm formation can be considered either desirable or undesirable phenomena and therefore an appropriately designed surface is required to facilitate or impede microbial adhesion to the surfaces[2].

Physicochemical properties of a surface play a significant role in microbial adhesion to surfaces[3] and therefore detailed analysis of the effect of these properties is required in order to develop a design methodology for antifouling applications.

Surface topography is recognized as a powerful tool for regulating many cell behaviors including adhesion and extensive study of the natural anti-biofilm surfaces reaffirms the importance of surface texture on anti-biofilm properties[4–6]. Although the study of the interaction of bacteria with textured surfaces has gained momentum in the recent years[7–15], the complex behavior of bacterial cell interacting with topographical features of textured surfaces has limited rigorous *quantitative* study of the "*state of adhesion*" of fouling organisms to textured surfaces.

In this study, polystyrene (PS) surfaces texturized with PS fibers were used as model surfaces with controlled topographies. Surface topography in form of nanofibers was selected for this study because it enables the study of the effect of surface curvature on bacteria-textured surface interaction in addition to the two commonly utilized

topographical parameters of feature size and spacing. *State of adhesion* of *Pseudomonas aeruginosa* (*P. aeruginosa*) bacteria to a broad range of fiber diameter (70-1100 nm) and spacing (sub 100 nm to microns) at *single-cell* level was analyzed and an energy-based approach was used to interpret the experimental data. Findings from this work will help advance the understanding of the fouling organism-surface interactions with the ultimate goal of controlling bacterial adhesion to the surfaces using topographical cues.

Chapter 2. Materials and methods

2-1. Materials

All materials and chemicals were purchased from Fisher Scientific (Pittsburgh, PA) unless otherwise noted. Polystyrene (PS) powder (Scientific Polymer, Ontario, NY) and xylene were used as received for fiber manufacturing. PS sheet (Goodfellow, Oakdale, PA) was cut into 3χ18 mm^2 rectangles and used as substrates in all experiments. Bacto Tryptone (17 g/L), Bacto Soytone (3 g/L), Dextrose (2.5 g/L), Sodium Chloride (5 g/L) and Dipotassium Phosphate (2.5 g/L) were dissolved in deionized (DI) water (Resistivity at 25 ˚C: 18.2 MΩ·cm) to prepare tryptic soy broth (TSB). 15 g/L of Bacto Agar was added to the TSB to make tryptic soy agar (TSA) plates. 9.84 g/L of Phosphate Buffered Saline (PBS) powder was dissolved in DI water to make PBS buffer. Polydimethylsiloxane (PDMS, SYLGARD® 184 elastomer) was prepared according to the manufacturer's instruction and was used to construct the holders utilized in the retention assay experiments. 10% electron microscopy grade glutaraldehyde (Electron Microscopy Sciences, Hatfield, PA) was diluted to a final concentration of 2.5% in DI water and was used for Scanning Electron Microscopy (SEM) sample preparation.

2-2. Nanofiber manufacturing

Highly aligned PS nanofibers were deposited on the PS substrates using the previously reported Spinneret based Tunable Engineered Parameters (STEP) technique[16], as schematically represented in Fig. 2-1.

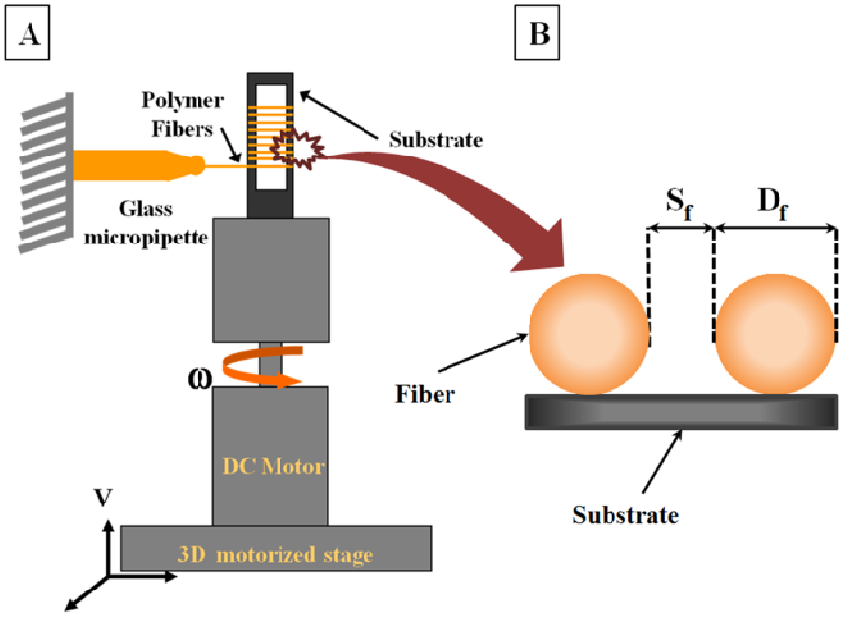

Figure 2-1. A: Schematic of the STEP platform for manufacturing of highly aligned polymeric nanofibers, B: Illustration of the geometrical parameters of diameter (D_f) and spacing (S_f) of the nanofibers.

Using this non-electrospinning method, nanofibers are formed by continuous pumping of PS/xylene solution through a micropipette spinneret (inner diameter: 100 µm, outer diameter 260 µm, Jensen Global, Santa Barbara, CA) using a syringe pump (Harvard Apparatus Inc., Holliston, MA) at a flow rate of 50-100 $\mu l.min^{-1}$. Rapid loss of solvent results in a solidified polymer nanofiber. For the work presented here, the PS substrate was mounted on a DC motor which in turn was mounted onto a motorized three degree of freedom micropositioning stage (VP-25XA, Newport Inc., Irvine, CA). Aligned PS nanofibers were deposited on the PS substrate by continuous pull-out of a polymeric solution filament from the extruded volume of the PS/xylene solution through the stainless steel microneedle.

The diameter of the manufactured fiber (D_f) was controlled by controlling the solution rheology through change of molecular weight or the concentration of the polymer in the polymer solution. The spacing between the fibers was controlled by controlling the linear velocity of the micropositioning stage (V) and the rotational speed of the DC motor (ω). The molecular weight and concentration of the polymer and the corresponding fiber diameters of small, medium, and large used in this study are shown in Table 2-1.

Table 2-1. The solution parameters for the small diameter (SD), medium diameter (MD) and large diameter (LD) nanofibers used in this work.

Name	Molecular weight (g/mol)	Concentration of PS in xylene (wt. %)	Diameter (nm)
SD	1 Million	7	91±17
MD	1.5 Million	7	482±52
LD	2 Million	13	971±151

2-3. Substrate characterization and preparation

The roughness of the substrates was measured using Atomic Force Microscopy (AFM) in order to demonstrate that the original roughness of the substrate is negligible compared with the size of the nanofibrous topographical features. Measurements were performed in tapping mode using a Veeco MultiMode AFM with NanoScope IVa controller and a TEFP cantilever. The roughness of the sample substrates were measured after depositing fibers on them and the results indicate that arithmetical mean roughness (R_a) of the PS substrate used in these experiments is 1.24 nm which is significantly less than the average

diameter of the smallest fibers (91 nm) used in this work.

A thin layer of the PS polymer solution used for manufacturing of the fibers was spin-coated on a Si wafer and used to measure the contact angle of the fiber material. 4.5 µl of deionized (DI) water and at least triplicate of each sample were used in all contact angle measurements. The contact angles of at least three droplets were captured on each sample at 25±1 ˚C using FTÅ 200 contact angle measurement system and angles were measured using the ImageJ software[17]. The results show that the PS of both substrate and fiber has the average contact angle of 91˚.

Prior to the retention assay experiments, all samples were gently washed once using 70% ethanol and rinsed twice with autoclaved DI water.

2-4. Bacterial cell culturing and retention assay

A 1.5% agar TSA plate was inoculated with *P. aeruginosa* PAO1 (Seattle *P. aeruginosa* PAO1 transposon mutant library, Seattle WA) from a -80 ˚C stock and the plate was subsequently incubated for 16 hours at 37 ˚C. A single colony was transferred from the plate into 10 mL of TSB in a 125 ml flask and incubated at 37˚C on a rotary shaker at 150 rpm for 5:30 hours. The resulting culture was diluted 200 times and transferred into a second TSB flask to grow at 37˚C on a rotary shaker at 97 rpm. Cells were harvested from the second culture on the exponential phase at OD_{600nm} = 0.3 by centrifugation (3000g, 11 minutes, 25±1 ˚C), resuspended in PBS, and presented on the samples.

To remove the effects of gravitational sedimentation on bacterial adhesion density, a PDMS holder was used to suspend the samples in bacterial suspension horizontally with the working area faced down. All holders were sterilized by soaking in DI water and autoclaving in liquid cycle.

Three different sets of experiments were carried out on three different days from three different cultures. In all experiments, triplicates of each sample were placed in bacterial suspension for 2.5 hours in a static system at 37˚C. Negative control experiments were run by soaking a holder and mounted sample in fresh TSB for 48 hours in the same conditions. All samples were fixed in 2.5% glutaraldehyde at 4˚C and dehydrated through serial ethanol washes at room temperature prior to SEM imaging.

2-5. Method of analysis

All samples were gold coated and imaged in high vacuum mode using a Scanning Electron Microscope (FEI Quanta 600 FEG, Hillsboro, OR). At least 150 images (magnification: 5000x) were captured along the centerline of the sample. Areas close to the edges were avoided.

Given the presence of all possible spacing values on the same sample, fibers may experience different spacing on their left and right side; therefore, in order to determine the modal and total adhesion densities for each combination, each fiber was considered as two half-fibers and cells interacting with more than one half-fiber were divided between them. The bacteria interacting with each half-fiber were counted manually and

categorized in AS (aligned with the spacing), CS (crossed the spacing), CF (crossed the fiber), and AF (aligned with the fiber) modes. Figure 2-2 provides several examples of the cell counting process.

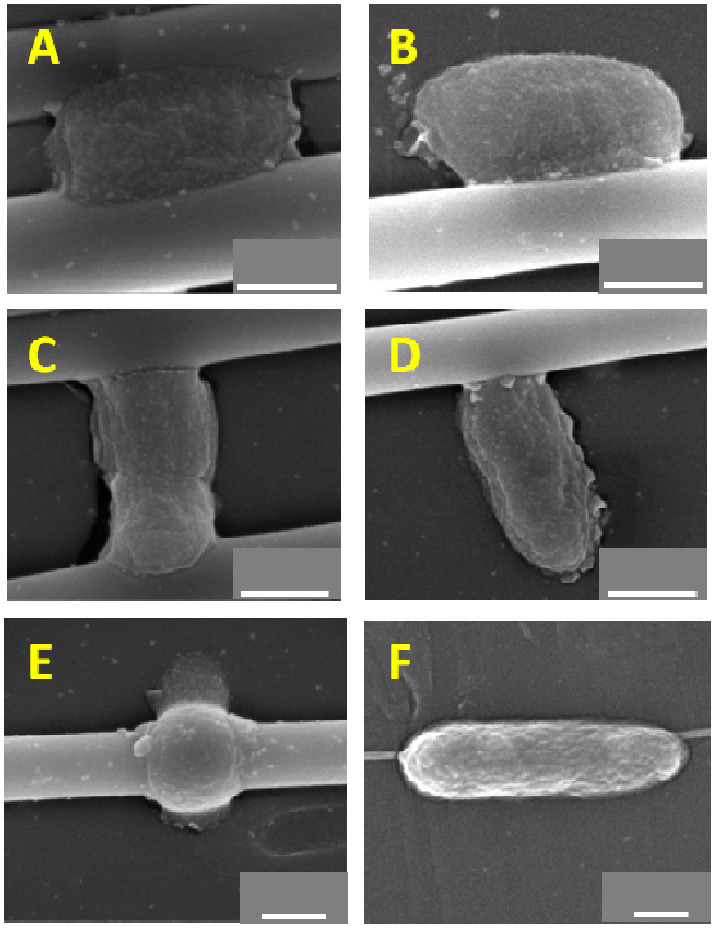

Figure 2-2. Examples of counting process A: half AS for each half-fiber, B: one AS for the half fiber, C: half CS for each half-fiber, D: one CS for the bottom half-fiber, E: half CF for each half fiber, F: half AF for each half fiber. All scale bars represent 500 nm.

In the counting process, the linear density was monitored after adding new data points to determine when the results reached stable points such that adding new data point would

not affect them (more than 5%).

2-6. Statistical and error analysis

Modal adhesion densities were reported as the mean number for the triplicate samples ± standard deviation. The statistical differences between different situations were analyzed using one way ANOVA test followed by a Tukey test. Distributions were considered significantly different at $p \leq 0.05$. For each combination of the fiber diameter and spacing, the total adhesion density was calculated as the summation of the modal densities and the error was calculated as the root mean square of the standard deviations of the modal adhesion densities.

Chapter 3. Controlling bacterial adhesion to surfaces using topographical cues: A study of the interaction of *Pseudomonas aeruginosa* with nanofiber-textured surfaces.

Pseudomonas aeruginosa PAO1, used as the model organism in this study, is a gram-negative, motile, rod-shaped (length (L_b) ≈ 1800 nm, diameter (D_b) ≈ 500 nm) bacterium that acts as an opportunistic human pathogen. Model surfaces with controlled topographical features were fabricated by depositing highly aligned PS nanofibers on flat PS substrates (arithmetic mean roughness: R_a < 2 nm) using the previously developed Spinneret based Tunable Engineered Parameters (STEP) technique[16] Given the diameter of the *P. aeruginosa*, three different fiber diameter (D_f) categories were defined: (1) small diameter (SD) fibers with $D_f < D_b$ with an average fiber diameter of 91±17 nm, (2) medium diameter (MD) fibers with $D_f \approx D_b$ with an average fiber diameter of 482±52 nm, and (3) large diameter (LD) fibers with $D_f > D_b$ and the average fiber diameter of 971±151 nm. Fibers from each diameter category were deposited at spacing varying from sub 100 nm to several microns, all on the same PS substrate. Considering the two main characteristic lengths of the bacteria body (L_b and D_b), the spacing between the fibers (defined as the edge to edge separation distance and shown as S_f in Fig. 3-1) was categorized according to the following: (1) $S_f < D_b$ (S_f < 300 nm), (2) $S_f \approx D_b$ (300 nm $\leq S_f \leq$ 600 nm), (3)

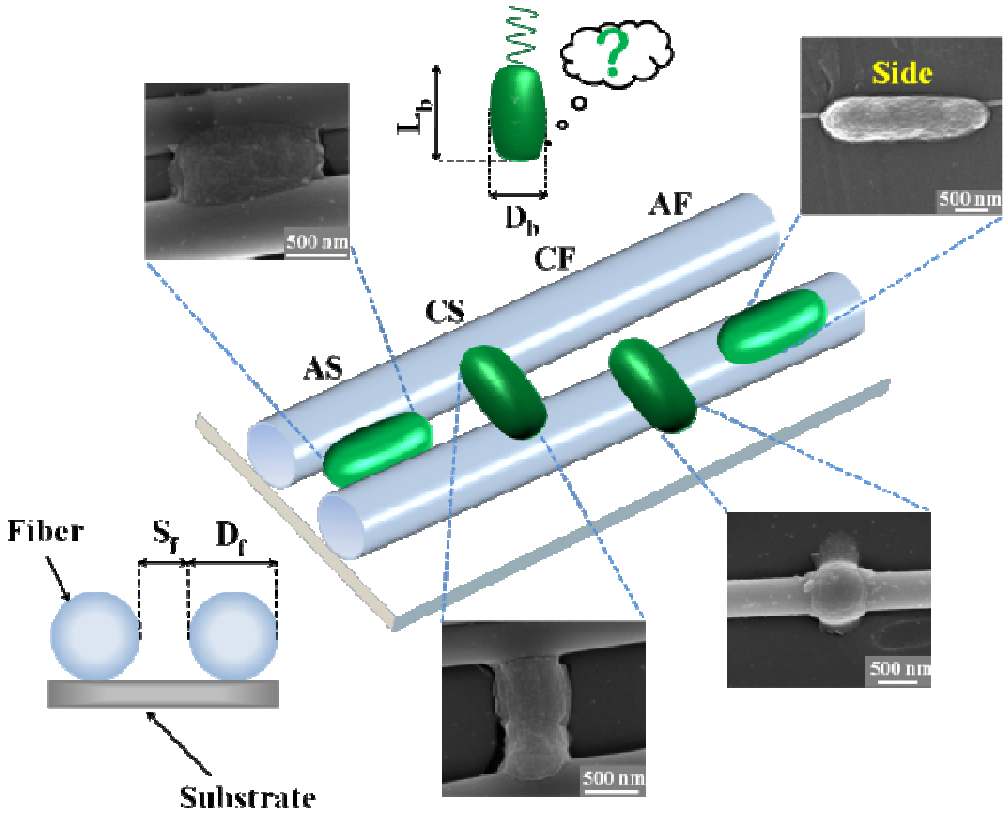

Figure 3-1. The two characteristic dimensions of the rod-shaped bacteria (length: L_b and diameter: D_b) and the two characteristic geometrical parameters of the nanofibers (spacing: S_f and diameter: D_f) result four dominant modes of adhesion: AS (aligned with the spacing), CS (crossed the spacing), CF (crossed the fiber), and AF (aligned with the fiber).

$D_b < S_f \leq L_b$: (600 nm $< S_f \leq$ 1800 nm), and (4) $S_f > L_b$ ($S_f >$ 1800 nm). Therefore, combinations of the topographical parameters of fiber diameter and spacing provide twelve possible surface topographical combinations for this study. Hereinafter, the nanofiber-coated PS substrates are referred to as samples.

The samples were submerged in the *P. aeruginosa* suspension (OD_{600nm}= 0.3) horizontally with the working area faced down in order to remove the effects of gravitational sedimentation on bacterial adhesion density. Retention assays were

conducted for 2.5 hours.

For all 12 combinations of the D_f and S_f the scanning electron microscopy (SEM) images were analyzed to quantify *total adhesion density* of bacteria defined as total number of bacteria/fiber length. Table 3-1 includes numerical values of the total adhesion density and their error. The effect of fiber diameter and spacing on the total adhesion density is shown in Fig. 3-2.

Table 3-1. Total adhesion density (number of cells/length of fiber (mm)) ± error as a function of fiber diameter (D_f) and spacing (S_f). Total adhesion density represents the adhesion density of all bacteria adhered to the surface regardless of their mode.

Diameter \ Spacing	$S_f < D_b$	$S_f \approx D_b$	$D_b < S_f \leq L_b$	$S_f > L_b$
$D_f < D_b$	15.2±1.8	20.6±5.3	20.8±2.9	29.1±6.6
$D_f \approx D_b$	8.3±1.1	19.5±2.0	25.7±5.4	44.7±5.7
$D_f > D_b$	14.7±1.4	33.4±3.3	42.7±8.1	83.0±5.8

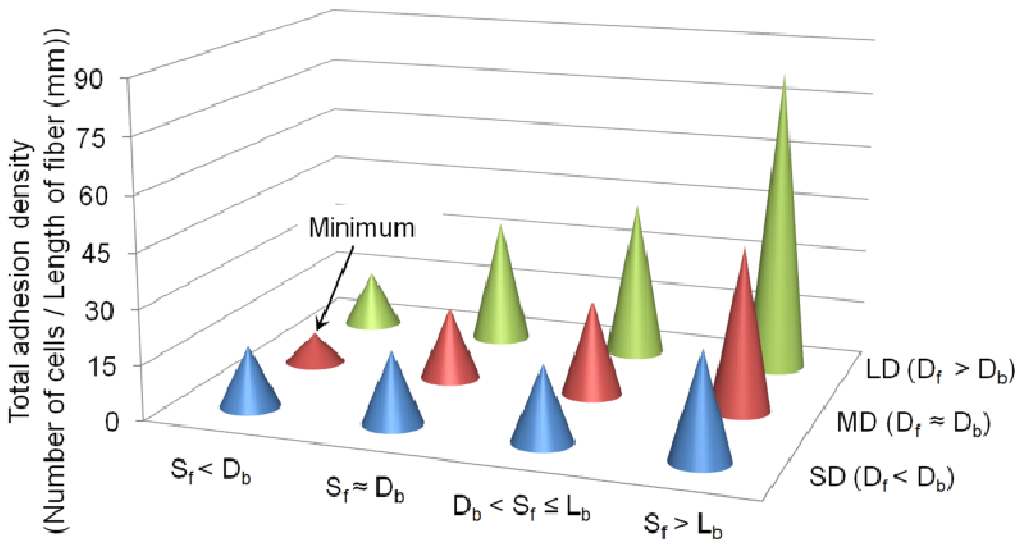

Figure 3-2. Distribution of the total adhesion density of bacteria to the PS nanofiber-textured surfaces as a function of fiber diameter (D_f) and spacing (S_f). The minimum value occurs for samples with medium diameter (MD) fibers at spacing less than the bacteria diameter ($S_f < D_b$).

The results demonstrate that the total adhesion density depends on both the topography size (fiber diameter) and spacing and has a minimum occurring for samples with MD fibers at spacing less than bacterial diameter ($S_f < D_b$).

In order to explain the reason behind these observations, the effect of surface topography size and spacing on the *state of adhesion* at single-cell level is investigated. Toward this goal, the samples were imaged using SEM and a quantitative analysis was performed. The observed states of adhesion of bacteria were categorized according to the following modes (Fig. 3-1): (1) Aligned with the spacing (AS): bacterium adheres in the spacing between the fibers and aligns itself with the fiber, (2) Crossed the spacing (CS): bacterium adheres in the spacing between the fibers while its long dimension is not

aligned with the fibers, (3) Crossed the fiber (CF) bacterium adheres on the fiber and its long dimension is not align with the fiber, and (4) Aligned with the fiber (AF): bacterium adheres on the fiber and aligns itself with the fiber. For each combination of the fiber diameter and spacing, the *modal adhesion density* of the bacteria (number of bacteria/fiber length) was calculated for each of the four modes. The experimental data in form of modal adhesion densities are presented in Fig. 3-3. The statistical analysis was conducted using one-way ANOVA followed by a Tukey test. Distributions were considered significantly different at $p \leq 0.05$. The AF mode data were not included in the figure as its adhesion density was consistently insignificant, when compared with the other modes.

Of particular interest is the modal adhesion density data for the spacing less than bacteria diameter ($S_f < D_b$) at which the minimum total adhesion density was observed. The effect of the fiber diameter (D_f) on the modal adhesion densities of the AS, CS, and CF are demonstrated in the top left subplot of the Fig. 3-3. From this figure, it can be seen that for the SD fibers, bacteria are most probable to cross the spacing between the fibers and adhere in the CS mode. Increasing the fiber diameter promotes the adhesion density of the bacteria aligned in the spacing between two fibers (AS mode) but conversely demotes the adhesion density of the CS mode such that the AS mode is the dominant mode of adhesion for both MD and LD samples. These trends result in the minimum total adhesion density (summation of the modal adhesion densities) for the MD fibers and emergence of a critical fiber diameter (D_{cr}) below which the preferred mode of adhesion changes from AS to the CS mode. Similar methodology may be followed for the other

three spacing categories demonstrated in Fig. 3-3. to determine the corresponding D_{cr} for each case. For brevity, we have limited the discussion to the optimum spacing of $S_f < D_b$.

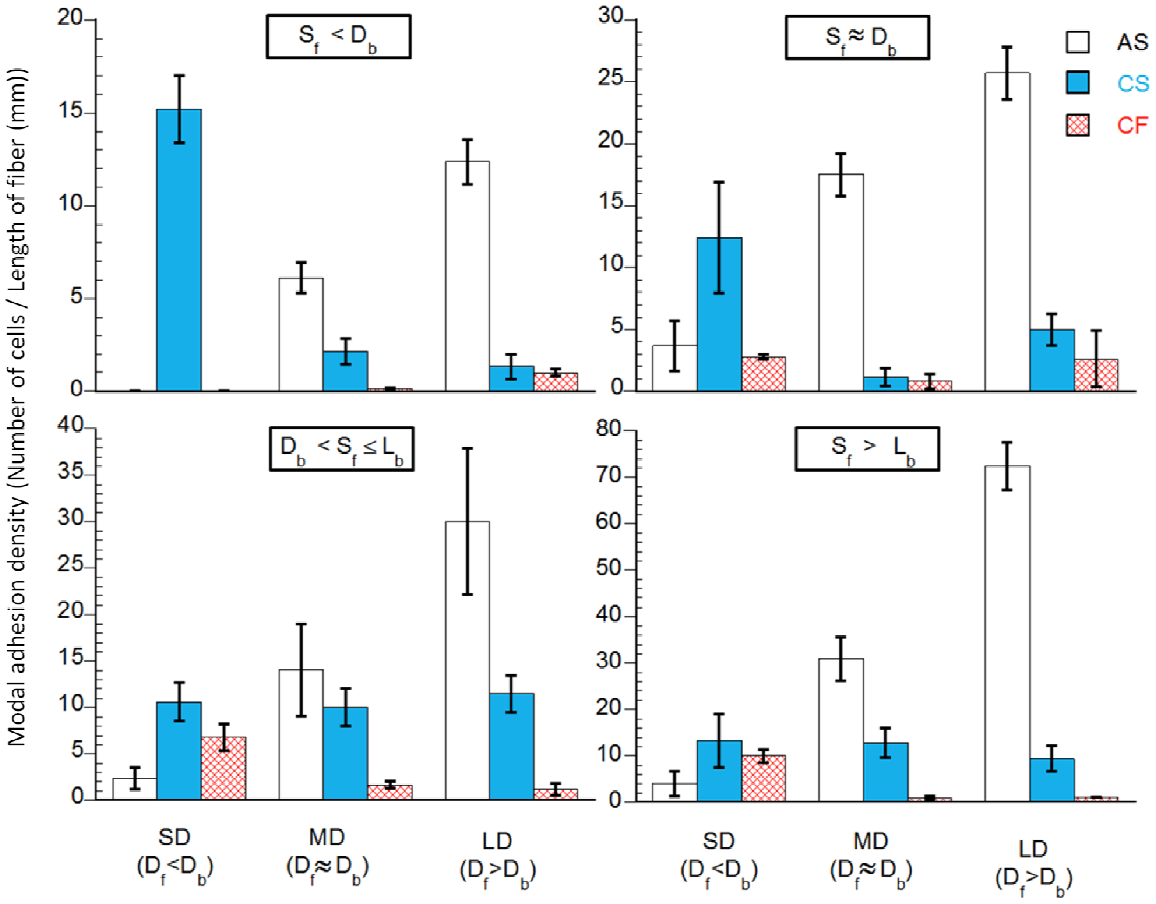

Figure 3-3. The effect of the fiber diameter (D_f) on the modal adhesion density of AS, CS, and CF modes (All modes of adhesion are illustrated in Fig. 3-1). Each subplot presents a range of the spacing (S_f). The fibers and substrates are both made of PS. Adhesion density in the AF mode was consistently insignificant, when compared with the other modes, therefore; it was not included in the figure.

Given the resemblance of the bacteria–textured surface interactions to the more widely

studied case of the vesicle–rigid surface interactions, we examine if the thermodynamics principles underlying the vesicle–rigid surface interactions can be used to explain the early stages of bacteria–textured surface interactions. It is known that a vesicle deforms upon contact with a rigid surface. Theoretically, the final shape of the vesicle and its state of adhesion can be predicted by minimizing the total free energy of adhesion[18]. The total free energy of adhesion (ΔG_{total}) results from the net balance of the gain and the cost of energy in the adhesion process. Gain in adhesion energy is attributed to the formation of the contact area (interface) (ΔG_A). Cost terms arise from the energy required for deformation (ΔG_D) which can be attributed to different sources such as the curvature energy associated with the bending the membrane, tension energy associated with the increase of the surface area, and the pressure energy associated with increase in volume. During the adhesion process, if the gain in energy becomes less than the cost then the adhesion is not thermodynamically favorable and it can only occur if an external source of energy compensates for the difference of the cost and gain.

Here, we investigate if this concept can be applied to interpret our experimental results on the interaction between the rigid cylindrical particle (fiber) and the cylindrical vesicle (bacterium). For instance, our experimental results for the AF mode show that regardless of the spacing between two fibers, this mode was never observed for MD fibers and was consistently insignificant for the other two fiber diameter categories. Figure 3-4 shows distribution of the AF modal adhesion density.

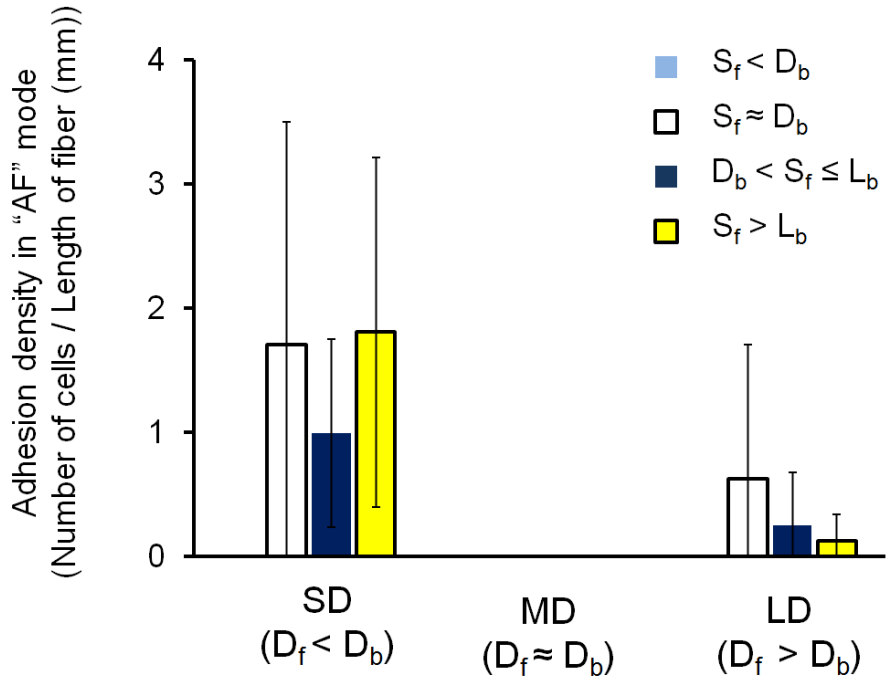

Figure 3-4. Adhesion density in the AF mode as a function of fiber diameter and spacing. Illustration of the AF mode, fiber diameter (D_f) and spacing (S_f) has been presented in Fig. 3-1.

Based on the aforementioned thermodynamic principles, this observation can be explained as reducing the fiber diameter increases the local curvature and consequently the cost of deformation, resulting in weak adhesion or desorption of the vesicle[19,20]. We observed adhesion in the AF mode for the LD fibers and not for the MD fibers, because the lower curvature of the LD fibers results in lower cost of deformation compared with the MD fiber. The AF mode was also observed for the SD fibers because the small diameter of SD fibers makes it possible for bacteria to interact with the flat substrate underneath the fibers and gain energy by adhesion to the flat substrate along sides of the fiber, as shown in the SEM image of the AF mode in Fig. 3.1. Nevertheless, adhesion in

the AF mode was rarely observed because in this mode bacteria will have to wrap around the fiber longitudinally and the cost of deformation is high.

The most detail analysis before current work used the fast Fourier transform (FFT) of the images of the bacterial cell population to predict the most probable orientation of cells[12,13,15] regardless of their binding site (spacing between features or features themselves). Following this method Edwards et al.[15] studied the interaction of *Thiobacillus caldus* with scratches on the surface of sulfide minerals and concluded that cells are likely to align themselves with the defects such that they gain more contact area. Edwards et al. hypothesized that this condition may allow cells to increase the binding energy. Using similar approach, another group[12,13] reported that the studied cells adhered in spacing between vertical nanopillars such that they achieve more contact area. These observations are in agreement with our observation presented here and can be interpreted as the tendency of the fouling organisms to maximize the first term (ΔG_A) of the presented model.

Here, the detailed analysis of the modal adhesion of bacteria to the nanofibrous structures has enabled us to demonstrate the importance of the topography curvature and its effect in regulating the cost of deformation (ΔG_D). Our finding suggests that an appropriate design of the topography is able to make the surface less favorable for adhesion by both reducing the available binding sites in all modes of adhesion and increasing the cost of deformation.

Based on the same thermodynamic principles, the minimum adhesion density should occur at spacing less than bacteria diameter as this is the only condition which eliminates direct contact of the cell with the flat substrate beneath the fibers in all modes of adhesion when combined with the LD or MD fibers (minimum gain in adhesion energy). For both of these topographical conditions AS is the dominant mode of adhesion. Reduction of the fiber diameter from LD to MD increases the curvature and reduces the size of the confined gap (confined gap refers to the area available at the intersection of two adjacent fibers ($S_f \lesssim 0$) as shown in Fig. 3-5). Therefore, these changes lower the possible gain in adhesion energy by raising the cost of deformation[1] and reducing the available binding sites for the adhesion in AS mode. Further reduction in the fiber diameter will results in lower adhesion energy until the critical fiber diameter (D_{cr}) that provides most energetically unfavorable condition for adhesion. Finding the intersection of the linear ($R^2 = 0.97$) and power law curves ($R^2 = 0.92$) fitted to the modal adhesion density of AS and CS respectively (top left subplot of Fig. 3-3), we estimate that this critical diameter would be $D_{cr} \lesssim 313$ nm, which is slightly smaller than bacteria diameter.

[1] AS mode is similar to the AF mode in that bacteria are longitudinally aligned and are in contact with two fibers when spacing is less than bacterial diameter.

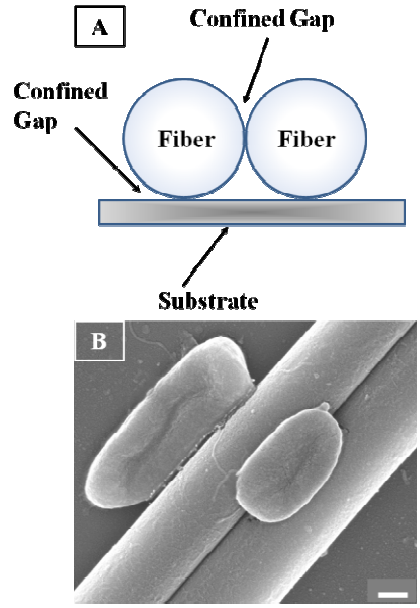

Figure 3-5. A: Illustration of the confined gap between fiber-fiber and fiber-substrate. B: SEM image shows cells adhered in AS mode (illustrated in Fig. 3-1) to the confined gap between fiber-fiber (S_f=0) and the fiber-substrate. The scale bar represents 200 nm.

For fiber diameters higher than D_{cr}, occurrence of the AS mode is more probable than the CS mode because adhesion in the CS mode is energetically more expensive. Reducing the fiber diameter to less than D_{cr} will promote adhesion in the CS mode, as it requires lower energy cost associated with deformation required for increasing the contact area[2].

[2] For spacing less than bacteria dimension competition is only between the AS and the CS modes, because adhesion in the two other modes is either geometrically unfeasible, or energetically highly expensive or both. Adhesion in CF mode to the SD fibers of spacing close to zero is an example of geometrical restriction which makes the CF mode completely impossible.

Conclusions and suggestions for future works

Bacterial adhesion is the first step in crucial pathogenic functions such as invasion and biofilms formation. Understanding the effect of the surface properties on microbial adhesion is a critical step toward designing antifouling surfaces. We have utilized nanofiber-textured model surfaces to study the effect of topographical feature size, spacing, and local curvature on the adhesion of bacteria at single-cell level. The thermodynamic principles governing the vesicle-rigid surface interactions were used to interpret the experimental data on the *state of adhesion* of bacteria and it was demonstrated that modal adhesion density data can be used towards designing anti-adhesion topographical geometry. Microbial adhesion to surfaces is a complex phenomenon and a variety of physicochemical and physiological properties of the cells such as dynamic and adaptive properties of the cell membrane and bacterial appendages play considerable roles in it[21]. Our observations suggest that the thermodynamic principles governing the vesicle–rigid surface interactions can be a useful tool for qualitative interpretation of the experimental data on the *state of adhesion* of bacteria to the textured surfaces at its early stages.

We conclude that texturizing the surface with appropriately designed local curvature is not only able to reduce the gain in adhesion process by providing less available binding sites (in all possible adhesion modes) but also through increasing the cost of deformation. The work presented here focused on better understanding of the adhesion of bacteria to the textured surfaces. In future, we will extend the current study by focusing on the effect of fibrous topographical features on biofilm formation stage.

References

1. Kargar, M., Wang, J., Nain, A. S. & Behkam, B. Controlling bacterial adhesion to surfaces using topographical cues: a study of the interaction of Pseudomonas aeruginosa with nanofiber-textured surfaces. *Soft Matter* **8**, 10254–10259 (2012).

2. Hori, K. & Matsumoto, S. Bacterial adhesion: From mechanism to control. *Biochemical Engineering Journal* **48**, 424–434 (2010).

3. Bos, R., Van der Mei, H. C. & Busscher, H. J. Physico-chemistry of initial microbial adhesive interactions - its mechanisms and methods for study. *Fems Microbiology Reviews* **23**, 179–230 (1999).

4. Ball, P. Engineering - Shark skin and other solutions. *Nature* **400**, 507–509 (1999).

5. Baum, C., Meyer, W., Stelzer, R., Fleischer, L. G. & Siebers, D. Average nanorough skin surface of the pilot whale (Globicephala melas, Delphinidae): considerations on the self-cleaning abilities based on nanoroughness. *Marine Biology* **140**, 653–657 (2002).

6. Scardino, A. J. & De Nys, R. Mini review: Biomimetic models and bioinspired surfaces for fouling control. *Biofouling* **27**, 73–86 (2011).

7. Whitehead, K. A., Colligon, J. & Verran, J. Retention of microbial cells in substratum surface features of micrometer and sub-micrometer dimensions. *Colloids and Surfaces B-Biointerfaces* **41**, 129–138 (2005).

8. Campoccia, D. *et al.* Study of Staphylococcus aureus adhesion on a novel nanostructured surface by chemiluminometry. *International Journal of Artificial Organs* **29**, 622–629 (2006).

9. Diaz, C., Schilardi, P. L., Salvarezza, R. C. & De Mele, M. F. L. Nano/Microscale order affects the early stages of biofilm formation on metal surfaces. *Langmuir* **23**, 11206–11210 (2007).

10. Chung, K. K. *et al.* Impact of engineered surface microtopography on biofilm formation of Staphylococcus aureus. *Biointerphases* **2**, 89–94 (2007).

11. Anselme, K. *et al.* The interaction of cells and bacteria with surfaces structured at the nanometre scale. *Acta Biomaterialia* **6**, 3824–3846 (2010).

12. Hochbaum, A. I. & Aizenberg, J. Bacteria pattern spontaneously on periodic nanostructure arrays. *Nano Letters* **10**, 3717–3721 (2010).

13. Epstein, A. K., Hochbaum, A. I., Kim, P. & Aizenberg, J. Control of bacterial biofilm growth on surfaces by nanostructural mechanics and geometry. *Nanotechnology* **22**, (2011).

14. Xu, L.-C. & Siedlecki, C. A. Submicron-textured biomaterial surface reduces staphylococcal bacterial adhesion and biofilm formation. *Acta Biomaterialia* **8**, 72–81 (2012).

15. Edwards, K. J. & Rutenberg, A. D. Microbial response to surface microtopography: the role of metabolism in localized mineral dissolution. *Chemical Geology* **180**, 19–32 (2001).

16. Nain, A. S., Sitti, M., Jacobson, A., Kowalewski, T. & Amon, C. Dry spinning based spinneret based tunable engineered parameters (STEP) technique for controlled and aligned deposition of polymeric nanofibers. *Macromolecular Rapid Communications* **30**, 1406–1412 (2009).

17. Stalder, A. F. *et al.* Low-bond axisymmetric drop shape analysis for surface tension and contact angle measurements of sessile drops. *Colloids and Surfaces a-Physicochemical and Engineering Aspects* **364**, 72–81 (2010).

18. Seifert, U. & Lipowsky, R. Adhesion of vesicles. *Physical Review A* **42**, 4768–4771 (1990).

19. Deserno, M. & Gelbart, W. M. Adhesion and wrapping in colloid-vesicle complexes. *Journal of Physical Chemistry B* **106**, 5543–5552 (2002).

20. Chen, J. Z. Y. & Mkrtchyan, S. Adhesion between a rigid cylindrical particle and a soft fluid membrane tube. *Physical Review E* **81**, (2010).

21. An, Y. H. & Friedman, R. J. Concise review of mechanisms of bacterial adhesion to biomaterial surfaces. *Journal of Biomedical Materials Research* **43**, 338–348 (1998).